Determination of the Free-Field Acoustic Radiation Characteristics of the Vibrating Plate Structures With Arbitrary Boundary Conditions

Łukasz J. Nowak
Department of Intelligent Technologies,
Institute of Fundamental Technological Research,
Polish Academy of Sciences,
ul. Pawinskiego 5B,
Warszawa 02-106, Poland
e-mail: lnowak@ippt.pan.pl

Tomasz G. Zieliński
Department of Intelligent Technologies,
Institute of Fundamental Technological Research,
Polish Academy of Sciences,
ul. Pawinskiego 5B,
Warszawa 02-106, Poland
e-mail: tzielins@ippt.pan.pl

The paper presents the developed algorithm which implements the indirect variational boundary element method (IVBEM) for computation of the free-field acoustic radiation characteristics of vibrating rectangle-shaped plate structures with arbitrary boundary conditions. In order to significantly reduce the computational time and cost, the algorithm takes advantage of simple geometry of the considered problem and symmetries between the elements. The procedure of determining the distribution of acoustic pressure is illustrated on the example of thin, rectangular plate with a part of one edge clamped and all other edges free. The eigenfrequencies and the corresponding vibrational mode shapes of the plate are computed using the finite element method (FEM). The results of the numerical simulations are compared to the results of the experiments carried out in an anechoic chamber, proving good agreement between the predictions and the observations. The reliability of simulations and high computational efficiency make the developed algorithm a useful tool in analysis of the acoustic radiation characteristics of vibrating plate structures. [DOI: 10.1115/1.4030214]

Keywords: acoustic radiation, indirect variational boundary element method, plate structures

1 Introduction

Active structural acoustic control of noise emitted by vibrating plate structures is a topic of great scientific interest for past several decades. The research in this field was initiated by Fuller and Silcox [1–3] and continued by Hansen and Snyder [4], Thi and Zuniga [5], Thomas et al. [6], Baumann et al. [7], and other researchers. The solutions to the problem are of great practical importance, as the considered phenomena can be used to describe many real-life mechanical systems [8]. In this context, computationally efficient mathematical methods and models that allow to link the parameters of vibrations of the considered structures with parameters of the generated acoustic pressure field in the ambient space are highly desirable. Most of the studies presented in literature consider only far-field acoustic radiation of baffled plates. In such case, the distribution of acoustic pressure field can be computed using Rayleigh's integral formula (for instance, see Ref. [9]). Such an approach is very convenient from the point of view of numerical computations; however, its experimental validation encounters many significant technical difficulties. This is especially true in case of structures with arbitrary boundary conditions, particularly nonuniform and including free edges. On the other hand, if the baffle is discarded from the considerations, the mathematical and numerical complexity of the relevant problem increases drastically. The present study addresses this issue by introducing an original, computationally effective algorithm for determining free-field acoustic radiation characteristics of rectangle-shaped, unbaffled plate structures with arbitrary boundary conditions.

The presence of the acoustic medium, which is necessary for acoustic waves to propagate, influences the vibrational characteristics of the considered structure, which is the source of the radiation. The problem of determining the eigenfrequencies and the corresponding modal shape functions of vibrating plate structures submerged in different media has been the topic of numerous scientific investigations (for example, see Refs. [10–14]), which resulted in the development of various computational methods and algorithms suitable for different systems and boundary conditions. Despite the fact that in many cases the influence of the acoustic medium cannot be neglected (this is particularly true for heavy fluids, such as water), if the vibrating thin plate structures are relatively small compared to the acoustic wavelength and the surrounding medium can be treated as a light fluid—such as, for example, air—then it can be shown [15] that in such case the eigenfrequencies and vibrational mode shapes of the plate are not significantly affected by the presence of the medium. This means that the mechanical analysis of the vibrational characteristics can be decoupled from the acoustic analysis and performed independently for the in vacuo case. Obtained results may be then used for the computation of the distribution of generated acoustic pressure by introducing them as the boundary conditions on the surface of the considered structure. Such an approach is used in the present study.

The present study concerns the free-field vibroacoustic emission of thin, rectangle-shaped plate structures. Analytical solutions describing either selected vibrational characteristics or parameters of the generated acoustic pressure field are known only for a limited number of some special cases of prescribed boundary conditions for such structures, like, for example, simply

Contributed by the Noise Control and Acoustics Division of ASME for publication in the Journal of Vibration and Acoustics. Manuscript received November 13, 2013; final manuscript received March 20, 2015; published online April 27, 2015. Assoc. Editor: Lonny Thompson.

supported, baffled plates [9,16,17]. In general case, such exact solutions cannot be given and the considered problem has to be solved numerically. Taking into account that the considered ambient medium is air, the eigenfrequencies and the corresponding vibrational mode shapes are determined independently from the acoustic analysis using the FEM. The acoustic pressure field distribution could also be computed using the same method (for example, see Refs. [18,19]) but it would require to expand the mesh of elements into a large area of space surrounding the vibrating plate and would significantly increase the computational cost. It would also require imposing special, absorbing boundary conditions in order to approximate the unbounded character of the considered domain. Several different approaches expanding the range of efficient applications of the FEM into the unbounded acoustic domains, such as *perfectly matched layers* or *infinite elements* exist. The detailed description of such methods can be found, for instance, in Refs. [20–22]. Acoustic radiation of baffled plates can be also analyzed using a fast multipole boundary element method [23]. The comparison between the computational efficiency of the FEM and the boundary element method in various acoustic problems falls beyond the scope of the present study, refer to Refs. [24–26] for details.

The boundary element method has been extensively developed since the 60s of the last century for purposes of various research and engineering fields. Some preliminaries of this method with examples of applications in mechanics, acoustics, and electromagnetics can be found in Refs. [27–30]. In the considered case of the free-field acoustic radiation of the thin, rectangular plate 2 of the specific features of the boundary element method make it particularly convenient to use. First, the dimension of the discretized domain is reduced by one, compared to the FEM model and includes only the flat surface of the plate. Second, the fundamental solution of the problem which is used for the formulation of the solved equations obeys the Sommerfeld radiation condition at infinity. This means that there is no need in implementing any additional computational techniques to take into account the unbounded character of the acoustic domain. On the other hand, some complexities in the computational process arise due to the fact that the considered problem is an exterior acoustic problem with open boundary surface for which the only applicable version of the chosen numerical method is the IVBEM [26]. The variational computational scheme introduces double surface integrals and highly singular terms to the solved equations. In the relevant literature, similar issues concerning plate structures have already been described (for example, see Ref. [31]); however, none of the sources include the detailed information about the implementation of the procedures for solving the derived equations. The importance of such information is associated with some significant simplifications that can be introduced at this stage by taking into account the simple geometry and some special features of the considered problem of a thin, rectangle-shaped, vibrating plate structure. For that reason, these important issues are included in the present study. The developed computational algorithm described herein takes advantage of the fact that the relevant IVBEM equations formulated for such a two-dimensional surface consist a huge number of terms, which values depend only on the geometry and mutual arrangement of pairs of boundary elements. Thus, it is possible to drastically reduce the required computational cost compared to direct implementation of the IVBEM method by using mapped meshes of identical elements and employing the occurring symmetries. The algorithm was implemented in MATLAB environment and proved its usefulness and efficiency in numerous performed computations. The obtained results of the numerical simulations compared to the results of the experimental investigations performed in an anechoic chamber are presented further. The present paper contains all the necessary information required for the straightforward reproduction of the developed computational scheme.

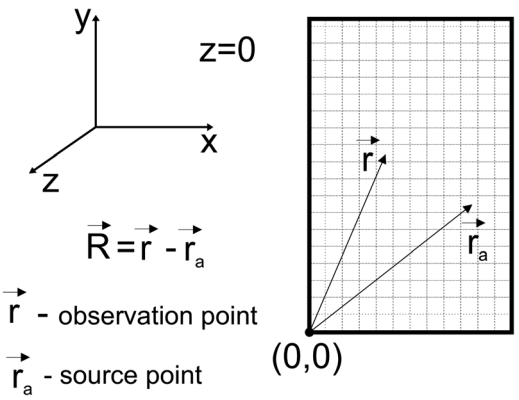

Fig. 1 The geometry of the considered problem: plate domain

2 Free-Field Acoustic Radiation—IVBEM Model

The geometry of the considered problem is presented in Fig. 1. It is assumed that the considered rectangular plate is positioned in the plane $z=0$ of the global XYZ coordinate system and that one of its edges has the coordinates (x,y) equal (0,0). The plate is thin and its thickness is neglected in further considerations. Due to the harmonic character of the considered excitation force and taking into account the fact that the system is linear and undamped, the acoustic pressure p at any point $\underline{\mathbf{r}}$ of the surrounding space satisfies the Helmholtz equation

$$\Delta p + k^2 p = 0 \tag{1}$$

where k is the wavenumber of the radiated acoustic wave and Δ is the Laplacian.

We solve Eq. (1) for Neumann boundary conditions imposed on the whole surface Ω of the considered plate

$$\left.\frac{\partial p}{\partial n}\right|_{(x,y)} = -\mathrm{i}\omega\rho_{\mathrm{a}} V_n(x,y) \quad \text{for } (x,y)\in\Omega \tag{2}$$

Here, $V_n(x,y)$ is the amplitude of the normal velocity of the surface of the plate at a point with coordinates (x,y), ω is the angular frequency of the radiated acoustic wave, and ρ_{a} is the density of air. For the sake of brevity the coordinates will be omitted in formulas presented further, unless they are important for clarity of the description. The distribution of the amplitude value of the normal velocity on the surface Ω is computed directly from the FEM model of plate vibrations and scaled to the results of measurements carried out using laser vibrometer.

The considered problem of the plate radiation in the free space is an exterior acoustic problem with an open boundary surface. It may be regarded as a special case of an exterior problem with closed boundary by considering both sides of the plate as separate surfaces denoted Ω^+ and Ω^-, where $\Omega=\Omega^+\cup\Omega^-$. We now introduce the following quantities:

- The single layer potential

$$\sigma\left(\underline{\mathbf{r}}_{\mathbf{a}}\right) = \frac{\partial p\left(\underline{\mathbf{r}}_{\mathbf{a}}^{+}\right)}{\partial n} - \frac{\partial p\left(\underline{\mathbf{r}}_{\mathbf{a}}^{-}\right)}{\partial n} \tag{3}$$

- The double layer potential

$$\mu\left(\underline{\mathbf{r}}_{\mathbf{a}}\right) = p\left(\underline{\mathbf{r}}_{\mathbf{a}}^{+}\right) - p\left(\underline{\mathbf{r}}_{\mathbf{a}}^{-}\right) \tag{4}$$

where r_a^+ and r_a^- denote the position of the acoustic point sources at surfaces Ω^+ and Ω^-, respectively. We can now rewrite the boundary conditions (2) as follows:

$$\frac{\partial p\left(\underline{\mathbf{r}}_{\mathbf{a}}^{-}\right)}{\partial n} = -\mathrm{i}\omega\rho_{\mathrm{a}} V_n\left(\underline{\mathbf{r}}_{\mathbf{a}}^{-}\right) \quad \text{on } \Omega^{-} \tag{5}$$

$$\frac{\partial p\left(\underline{\mathbf{r}}_{\mathbf{a}}^{+}\right)}{\partial n} = -\mathrm{i}\omega\rho_{\mathrm{a}} V_n\left(\underline{\mathbf{r}}_{\mathbf{a}}^{+}\right) \quad \text{on } \Omega^{+} \tag{6}$$

By assuming for thin plate $\Omega^{+} \approx \Omega^{-} \approx \Omega$ and substituting Eqs. (5) and (6) into Eq. (3), we obtain

$$\sigma = 0 \quad \text{and} \quad \frac{\partial p}{\partial n} = -\mathrm{i}\omega\rho V_n \quad \text{on } \Omega \tag{7}$$

The acoustic pressure at any point of the ambient space indicated by a vector $\underline{r}$ is described with the following boundary integral formulation [26]:

$$p(\underline{\mathbf{r}}) = \int_{\Omega} \mu(\underline{\mathbf{r}}_{\mathbf{a}}) \frac{\partial G(\underline{\mathbf{r}}, \underline{\mathbf{r}}_{\mathbf{a}})}{\partial n} d\Omega(\underline{\mathbf{r}}_{\mathbf{a}}) \tag{8}$$

where G is the Green's function, which satisfies following equation:

$$\Delta G(\underline{\mathbf{r}}, \underline{\mathbf{r}}_{\mathbf{a}}) + k^2 G(\underline{\mathbf{r}}, \underline{\mathbf{r}}_{\mathbf{a}}) = \delta(\underline{\mathbf{r}}, \underline{\mathbf{r}}_{\mathbf{a}}) \tag{9}$$

where $\delta(\underline{\mathbf{r}}, \underline{\mathbf{r}}_{\mathbf{a}})$ denotes the Dirac delta function. The considered fundamental solution should also satisfy the Sommerfeld radiation condition

$$\lim_{|\underline{\mathbf{r}}-\underline{\mathbf{r}}_{\mathbf{a}}|\to\infty} |\underline{\mathbf{r}} - \underline{\mathbf{r}}_{\mathbf{a}}| \left(\frac{\partial G(\underline{\mathbf{r}}, \underline{\mathbf{r}}_{\mathbf{a}})}{\partial |\underline{\mathbf{r}} - \underline{\mathbf{r}}_{\mathbf{a}}|} + \mathrm{i}kG(\underline{\mathbf{r}}, \underline{\mathbf{r}}_{\mathbf{a}}) \right) = 0 \tag{10}$$

Fulfillment of the condition (10) ensures that the obtained solution is valid for the free-field acoustic environment. The considered Green's function in the three-dimensional space has the form

$$G(\underline{\mathbf{r}}, \underline{\mathbf{r}}_{\mathbf{a}}) = \frac{e^{-\mathrm{i}k|\underline{\mathbf{r}}-\underline{\mathbf{r}}_{\mathbf{a}}|}}{4\pi|\underline{\mathbf{r}} - \underline{\mathbf{r}}_{\mathbf{a}}|} \tag{11}$$

By taking into account the boundary conditions (7), the integral equation (8) can be rewritten as

$$-\mathrm{i}\omega\rho V_n = \int_{\Omega} \mu(\underline{\mathbf{r}}_{\mathbf{a}}) \frac{\partial^2 G(\underline{\mathbf{r}}, \underline{\mathbf{r}}_{\mathbf{a}})}{\partial n(\underline{\mathbf{r}}) \partial n(\underline{\mathbf{r}}_{\mathbf{a}})} d\Omega(\underline{\mathbf{r}}_{\mathbf{a}}) \tag{12}$$

Equation (12) has to be solved for the unknown double layer potential μ on Ω. To this end, the equivalent variational statement is used, namely, the solution μ will minimize the following functional [26]:

$$\mathcal{J} = 2\int_{\Omega} \mathrm{i}\omega\rho\mu(\underline{\mathbf{r}}) V_n(\underline{\mathbf{r}}) + \int_{\Omega}\int_{\Omega} \mu(\underline{\mathbf{r}})\mu(\underline{\mathbf{r}}_{\mathbf{a}}) \frac{\partial^2 G(\underline{\mathbf{r}}, \underline{\mathbf{r}}_{\mathbf{a}})}{\partial n(\underline{\mathbf{r}}) \partial n(\underline{\mathbf{r}}_{\mathbf{a}})} d\Omega(\underline{\mathbf{r}}) d\Omega(\underline{\mathbf{r}}_{\mathbf{a}}) \tag{13}$$

The properties of the Green's function and the continuity of μ allow to rewrite the second, highly singular integral in an equivalent, less singular form, better suited for numerical calculations

$$\int_{\Omega}\int_{\Omega} \mu(\underline{\mathbf{r}})\mu(\underline{\mathbf{r}}_{\mathbf{a}}) \frac{\partial^2 G(\underline{\mathbf{r}}, \underline{\mathbf{r}}_{\mathbf{a}})}{\partial n(\underline{\mathbf{r}}) \partial n(\underline{\mathbf{r}}_{\mathbf{a}})} d\Omega(\underline{\mathbf{r}}) d\Omega(\underline{\mathbf{r}}_{\mathbf{a}}) = \int_{\Omega}\int_{\Omega} G(\underline{\mathbf{r}}, r_a) \Big[k^2 \mu(\underline{\mathbf{r}})\mu(\underline{\mathbf{r}}_{\mathbf{a}}) \left(\underline{\mathbf{n}}(\underline{\mathbf{r}}) \cdot \underline{\mathbf{n}}(\underline{\mathbf{r}}_{\mathbf{a}})\right) - (\nabla \times \mu(\underline{\mathbf{r}})) \cdot (\nabla \times \mu(\underline{\mathbf{r}}_{\mathbf{a}})) \Big] d\Omega(\underline{\mathbf{r}}) d\Omega(\underline{\mathbf{r}}_{\mathbf{a}}) \tag{14}$$

where

$$\nabla \times \mu = \underline{\mathbf{n}} \times \underline{\nabla}\mu \tag{15}$$

and $\underline{\mathbf{n}}$ is the unit vector normal to the surface of the boundary plate.

The considered area Ω is discretized into a number n_e of small boundary elements with corresponding areas $\Omega^e, e \in \{1, 2, \ldots, n_e\}$ and n_n nodes defined at some particular locations of the elements. n_{en} is the number of nodes belonging to a single element. Note that the elements may (and usually do) share common nodes, so, in general, $n_n \neq n_e n_{en}$. It is assumed, that the sought double layer potential at every single element can be approximated by a product of the unknown nodal values μ_i and the element shape functions N_i^e (which take the value of one in the corresponding node i and are zero in every other nodes), namely,

$$\mu(\underline{\mathbf{r}}) \approx \hat{\mu}(\underline{\mathbf{r}}) = \sum_{i=1}^{n_{en}} N_i^e(\underline{\mathbf{r}})\mu_i \quad (\underline{\mathbf{r}} \in \Omega^e) \tag{16}$$

The discretized form of the functional (13) can be now written as

$$\mathcal{J} = \sum_{i=1}^{n_n}\sum_{j=1}^{n_n} \mu_i B_{ij} \mu_j - 2\sum_{i=1}^{n_n} \mu_i C_i \tag{17}$$

where

$$B_{ij} = \int_{\Omega_i}\int_{\Omega_j} G(\underline{\mathbf{r}}, \underline{\mathbf{r}}_{\mathbf{a}}) [k^2 N_i(\underline{\mathbf{r}}) N_j(\underline{\mathbf{r}}_{\mathbf{a}}) - (\underline{\nabla} N_i(\underline{\mathbf{r}}) \times \underline{\mathbf{n}}) \cdot (\underline{\nabla} N_j(\underline{\mathbf{r}}_{\mathbf{a}}) \times \underline{\mathbf{n}})] d\Omega_i(\underline{\mathbf{r}}) d\Omega_j(\underline{\mathbf{r}}_{\mathbf{a}}) \tag{18}$$

and

$$C_i = -\mathrm{i}\omega\rho V_n^i \int_{\Omega_i} N_i(\underline{\mathbf{r}}) d\Omega_i(\underline{\mathbf{r}}) \tag{19}$$

where V_n^i denotes the normal velocity at point i. The global shape functions $N_i(\underline{\mathbf{r}})$ are defined in the whole boundary surface Ω. Inside every element to which node i belongs functions N_i are identical to the corresponding local shape functions N_i^e and are zero in all other domains. Thus, the integration surfaces Ω_i and Ω_j include all of the elements that contain interpolation nodes i and j, respectively.

To find the double layer potential values in the specified nodes using the variational scheme the following equation is solved:

$$\frac{\partial \mathcal{J}}{\partial \mu} = 0 \tag{20}$$

which yields

$$\underline{\underline{\mathbf{B}}}\,\underline{\boldsymbol{\mu}} = \underline{\mathbf{C}} \tag{21}$$

where $\underline{\underline{\mathbf{B}}}$ is the $(n_n \times n_n)$ size matrix composed of elements B_{ij} described by relation (18), $\underline{\mathbf{C}}$ is the $(n_n \times 1)$ vector composed of elements C_i described by relation (19) and $\underline{\boldsymbol{\mu}}$ is the $(n_n \times 1)$ vector of unknown nodal values of the double layer potential.

Now, the acoustic pressure in any point of the ambient space is given by the following relation:

$$p(\underline{\mathbf{r}}) = \underline{\mathbf{D}}^{\mathrm{T}}\underline{\boldsymbol{\mu}} \tag{22}$$

where the elements of vector $\underline{\mathbf{D}}$ are given with the following formula [26]:

$$D_i = \int_{\Omega} N_i(\underline{\mathbf{r}}_a) \frac{\partial G(\underline{\mathbf{r}}, \underline{\mathbf{r}}_a)}{\partial \underline{\mathbf{n}}(\underline{\mathbf{r}}_a)} d\Omega(\underline{\mathbf{r}}_a) \tag{23}$$

Assuming that the observation point indicated by the vector $\underline{\mathbf{r}}$ has coordinates (x, y, z) and the source point on the plate indicated by the vector $\underline{\mathbf{r}}_a$ has coordinates $(x_a, y_a, 0)$, the normal derivative of the Green's function is equal

$$\frac{\partial G(\underline{\mathbf{r}}, \underline{\mathbf{r}}_a)}{\partial \underline{\mathbf{n}}(\underline{\mathbf{r}}_a)} = z e^{-ik\sqrt{(x-x_a)^2+(y-y_a)^2+z^2}} \cdot \frac{-1 - ik\sqrt{(x-x_a)^2+(y-y_a)^2+z^2}}{\left(\sqrt{(x-x_a)^2+(y-y_a)^2+z^2}\right)^3} \tag{24}$$

After solving Eq. (21) with the coefficients of Eqs. (18) and (19) for the unknown nodal values μ_i of the double layer potential in the whole considered plate domain Ω, Eq. (22) is solved only for those points of the ambient space in which the values of acoustic pressure are sought.

3 Model Implementation

The developed algorithm for computation of the free-field acoustic radiation characteristics of the vibrating rectangular plate has been tailored to exploit the simple geometry of the considered problem (see Fig. 1). The domain Ω is divided into n_e identical, first-order rectangular boundary elements. The elements are arranged in n_{row} rows and n_{col} columns. The resolution of the division can be adapted to the considered form of vibrations with an adequate reserve as the computation time and cost will be significantly reduced by taking the advantage of the occurring symmetries. Inside every single element a local coordinate system $(\xi, \eta), \xi \in \langle -1; 1\rangle, \eta \in \langle -1; 1\rangle$ with axes parallel to the X- and Y-axes of the global coordinate system, respectively.

The application of linear shape functions definitely ensures the convergence of solution, as they satisfy the completeness and compatibility conditions for the considered problem [26]. The chosen functions defined for any boundary element e are as follows:

$$\begin{aligned} N_1^e(\xi,\eta) &= \frac{1}{4}(1-\xi)(1-\eta) \\ N_2^e(\xi,\eta) &= \frac{1}{4}(1+\xi)(1-\eta) \\ N_3^e(\xi,\eta) &= \frac{1}{4}(1+\xi)(1+\eta) \\ N_4^e(\xi,\eta) &= \frac{1}{4}(1-\xi)(1+\eta) \end{aligned} \tag{25}$$

Based on the chosen element shape functions and taking into account, the fact that due to the considered geometry and mesh properties a single interpolation node can belong to one, two, or four neighboring boundary elements, the coefficients B_{ij}, C_i, and D_i are computed using Eqs. (18), (19), and (24). The surface integrals are determined numerically using four-point Gauss integration scheme, except for the cases in which the integration surfaces overlap over the same boundary element. In such situation, results obtained with the standard numerical method would be burdened with significant error due to singularities in the integrand. To avoid this obstacle, the special algorithm for dealing with such double surface integrals with $1/R$ singularity proposed by Wang and Atalla [31,32] has been implemented. The algorithm is briefly described below.

Taking into account the form of the Green's function for the considered problem, given with Eq. (11) and transforming Eq. (18) into the local coordinate system, the double surface integral over the same boundary element may be expressed as follows:

$$\begin{aligned} &\int_{\Omega_i^e}\int_{\Omega_j^e} G(\underline{\mathbf{r}}, \underline{\mathbf{r}}_a)[k^2 N_i^e(\underline{\mathbf{r}}) N_j^e(\underline{\mathbf{r}}_a) \\ &\quad - (\underline{\nabla} N_i^e(\underline{\mathbf{r}}) \times \underline{\mathbf{n}}) \cdot \left(\underline{\nabla} N_j^e(\underline{\mathbf{r}}_a) \times \underline{\mathbf{n}}\right)] d\Omega_i^e(\underline{\mathbf{r}}) d\Omega_j^e(\underline{\mathbf{r}}_a) \\ &\quad = \int_{-1}^{1}\int_{-1}^{1}\int_{-1}^{1}\int_{-1}^{1} \frac{e^{-ik|\underline{\mathbf{r}}-\underline{\mathbf{r}}_a|}}{4\pi|\underline{\mathbf{r}}-\underline{\mathbf{r}}_a|}[k^2 N_i^e(\underline{\mathbf{r}}) N_j^e(\underline{\mathbf{r}}_a) \\ &\quad\quad - (\underline{\nabla} N_i^e(\underline{\mathbf{r}}) \times \underline{\mathbf{n}}) \cdot \left(\underline{\nabla} N_j^e(\underline{\mathbf{r}}_a) \times \underline{\mathbf{n}}\right)] J_i J_j d\xi_i d\eta_i d\xi_j d\eta_j \end{aligned} \tag{26}$$

where J_i and J_j are the Jacobians of the transformation of the local coordinate system to the global coordinate system which satisfy the following relation:

$$d\Omega_i^e = J_i d\xi_i d\eta_i, \quad d\Omega_j^e = J_j d\xi_j d\eta_j \tag{27}$$

Taking into account the considered geometry

$$J_i = J_j = \frac{a^e b^e}{4} \tag{28}$$

where a^e and b^e are the lengths of edges of the rectangular boundary element e parallel to the X- and Y-axis of the global coordinate system, respectively. Equation (26) can now be rewritten in the following form:

$$\begin{aligned} &\int_{-1}^{1}\int_{-1}^{1}\int_{-1}^{1}\int_{-1}^{1} \frac{e^{-ik(\underline{\mathbf{r}}-\underline{\mathbf{r}}_a)}}{4\pi|\underline{\mathbf{r}}-\underline{\mathbf{r}}_a|}[k^2 N_i^e(\underline{\mathbf{r}}) N_j^e(\underline{\mathbf{r}}_a) \\ &\quad - (\underline{\nabla} N_i^e(\underline{\mathbf{r}}) \times \underline{\mathbf{n}}) \cdot \left(\underline{\nabla} N_j^e(\underline{\mathbf{r}}_a) \times \underline{\mathbf{n}}\right)] J_i J_j d\xi_i d\eta_i d\xi_j d\eta_j \\ &\quad = \int_{-1}^{1}\int_{-1}^{1}\int_{-1}^{1}\int_{-1}^{1} \frac{f(\xi_i, \eta_i, \xi_j, \eta_j)}{r^e} d\xi_i d\eta_i d\xi_j d\eta_j \end{aligned} \tag{29}$$

where

$$\begin{aligned} f(\xi_i, \eta_i, \xi_j, \eta_j) = \frac{e^{-ikR}}{4\pi}&[k^2 N_i^e(\underline{\mathbf{r}}) N_j^e(\underline{\mathbf{r}}_a) \\ &- (\underline{\nabla} N_i^e(\underline{\mathbf{r}}) \times \underline{\mathbf{n}}) \cdot \left(\underline{\nabla} N_j^e(\underline{\mathbf{r}}_a) \times \underline{\mathbf{n}}\right)] J_i J_j \frac{r^e}{R} \end{aligned} \tag{30}$$

and

$$R = |\underline{\mathbf{R}}| = |\underline{\mathbf{r}} - \underline{\mathbf{r}}_a| = \sqrt{(x_i - x_j)^2 + (y_i - y_j)^2} \tag{31}$$

$$r^e = \sqrt{(\xi_i - \xi_j)^2 + (\eta_i - \eta_j)^2} \tag{32}$$

The integration variables are converted as follows:

$$x_i = x_p + \frac{a^e(1+\xi_i)}{2} \tag{33}$$

$$x_j = x_p + \frac{a^e(1+\xi_j)}{2} \tag{34}$$

$$y_i = y_p + \frac{b^e(1+\eta_i)}{2} \tag{35}$$

$$y_j = y_p + \frac{b^e(1+\eta_j)}{2} \tag{36}$$

where (x_p, y_p) are coordinates of the center point of element e. Therefore

$$R(\xi_i,\eta_i,\xi_j,\eta_j)=\sqrt{\left[\frac{a^e}{2}(\xi_i-\xi_j)\right]^2+\left[\frac{b^e}{2}(\eta_i-\eta_j)\right]^2} \tag{37}$$

The integral (29) is computed using four-point numerical scheme described in Ref. [32]

$$\int_{-1}^{1}\int_{-1}^{1}\int_{-1}^{1}\int_{-1}^{1}\frac{f(\xi_i,\eta_i,\xi_j,\eta_j)}{r^e}d\xi_i d\eta_i d\xi_j d\eta_j = \sum_{m=1}^{M_m}\sum_{n=1}^{M_n}\sum_{o=1}^{M_o}\sum_{p=1}^{M_p} f(\xi_m,\eta_n,\xi_o,\eta_p)W_{mnop} \tag{38}$$

where

$$M_m=M_n=M_o=M_p=4 \tag{39}$$

denote the Wang's integration order. The values of weight coefficients W_{mnop} and the coordinates of the integration points ξ_m, η_n, ξ_o, η_p are given in Ref. [32].

The proposed algorithm for determination of the free-field acoustic radiation characteristics of the vibrating plate structure includes the following steps:

(1) Generation of mesh consisting of identical, rectangular elements covering the whole surface of the considered plate with a given resolution.
(2) Interpolation of values of the normal velocities in the nodes basing on the scaled results of the FEM analysis of the eigenvalue problem for the considered plate.
(3) Computation of the elements of matrix $\underline{\underline{\mathbf{B}}}$ and vectors $\underline{\mathbf{C}}$ and $\underline{\mathbf{D}}$ using formulas (18), (19), (23), and (24).
(4) Solution of Eq. (21) for the unknown double layer potential values in the interpolation nodes.
(5) Solution of Eq. (22) for the unknown values of the acoustic pressure in selected points of the ambient space.
(6) Postprocessing and visualization of the results.

Note that step 3 is crucial from the point of view of the computational time and cost. It involves each with each element double surface integrals for every corresponding interpolation node to compute the coefficients B_{ij} and for that reason it is the bottleneck of the whole process, as the number of the required operations increases dramatically with increasing resolution of discretization. Moreover, due to the fact that the coefficients B_{ij} are frequency-dependent this step of the algorithm has to be repeated for every single considered frequency of vibrations. Thus, it is highly desirable to reduce the duration of this step as possible. The following features concerning this problem should be taken into account:

- The Green's function for the considered problem (11) is symmetrical with respect to its arguments $\underline{\mathbf{r}}$ and $\underline{\mathbf{r_a}}$;
- the unit vector $\underline{\mathbf{n}}$ is constant on the whole surface of the boundary plate;
- the Jacobians (28) are equal for all elements; and
- the values of the double surface integral over a single boundary element (29) concerning the same pairs of the shape functions are equal for all elements of the mesh.

Based on the observations mentioned above, two important conclusions regarding the solved equations may be derived. The first, quite obvious, attribute of the matrix $\underline{\underline{\mathbf{B}}}$ that should be noticed is that it is symmetrical. This property actually results from the variational formulation used for the problem and is common for all IVBEM based models. The symmetry of the matrix allows to reduce the number of the computed elements; however, the overall computational cost is still high as the number of required operations increases rapidly with increasing resolution (n_e) of discretization. More significant reduction of the computational time and cost may be obtained by taking advantage of the simple geometry of the plate domain and the properties of the regular mesh of elements. The second important conclusion is that the value of the double surface integral over two surfaces of the boundary elements in Eq. (18) in the considered case depends only on the absolute distance between the elements.

Based on the above observations and conclusions, the following algorithm for computation of the elements of matrix $\underline{\underline{\mathbf{B}}}$ given with Eq. (18) is proposed:

(1) A single mesh element $s, 1 \le s \le n_e$, in the corner of the rectangular domain is chosen. The values of the following expression are computed for all mesh elements $e, e \in \{1,2,\ldots,n_e\}$ and for all possible pairs of the element shape functions $(N_i^s, N_j^e), i \in \{1,\ldots,4\}, j \in \{1,\ldots,4\}$:

$$\int_{\Omega^s}\int_{\Omega^e} G(\underline{\mathbf{r}},\underline{\mathbf{r_a}})\left[k^2 N_i^s(\underline{\mathbf{r}})N_j^e(\underline{\mathbf{r_a}}) - (\underline{\nabla} N_i^s(\underline{\mathbf{r}})\times\underline{\mathbf{n}})\cdot(\underline{\nabla} N_j^e(\underline{\mathbf{r_a}})\times\underline{\mathbf{n}})\right] d\Omega^s(\underline{\mathbf{r}})d\Omega^e(\underline{\mathbf{r_a}}) \tag{40}$$

The results are stored in memory. In the case when $s=e$ the described above four-point special integration scheme (26) is used to deal with singularities.
(2) For every pair of the mesh interpolation nodes with indices $(i,j), i \in \{1,\ldots,n_n\}, j \in \{1,\ldots,i\}$ the numbers of the boundary elements to which the nodes belong, distance between the elements and the corresponding numbers of the element shape functions are determined. The adequate values of the expression (40) computed in the previous step of the algorithm are loaded from the memory and added to the values of the corresponding elements B_{ij}.
(3) Using the symmetry property of the matrix $\underline{\underline{\mathbf{B}}}$ the values from the upper diagonal part are copied to the corresponding elements in the lower diagonal part.

The first step of the algorithm requires $n_{en}^2 n_n$ times computation of the double surface integral given by the expression (40). The two following steps are computationally cheap and do not affect significantly the total duration of the process. In case if only the symmetry property of the matrix $\underline{\underline{\mathbf{B}}}$ was used the complexity of the algorithm would be $O(n_{en}^2 n_n^2)$. Taking into account the fact that in practical applications $n_{en} \ll n_n$ and the total number of interpolation nodes is usually of the order 10^2 or greater the savings of computational time and cost associated with the use of the presented algorithm is significant.

The developed algorithm has been implemented using the MATLAB environment and tested on a standard personal computer with 4-core processor. The total computational time of determining the value of acoustic pressure in a single point of space was less than 1 min for a mesh consisting of one thousand elements.

4 Experimental Investigations, Results, and Discussion

The experimental investigations regarding the free-field acoustic radiation characteristics have been carried out in an anechoic chamber using 20 cm wide, 30 cm high, and 1 mm thick rectangular plate made of aluminum. The plate was clamped in the central part of one of its shorter edges while all other edges were free, as presented in Fig. 2.

The plate was excited to vibrate by a pair of piezoelectric transducers, mounted symmetrically on both sides of the structure and driven with reversely polarized harmonic voltage signal from an amplifier connected to a generator. Low-order vibrational modes with corresponding eigenfrequencies up to 400 Hz were examined. The plate revealed sharp resonant characteristics and acoustic radiation for off-resonant frequencies turned out to be very low.

The amplitude of the acoustic pressure in selected points of ambient space was measured using half-inch condenser

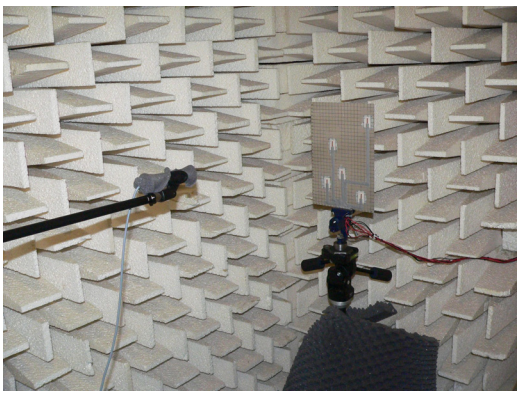

Fig. 2 Aluminum plate structure used in the experimental investigations in an anechoic chamber

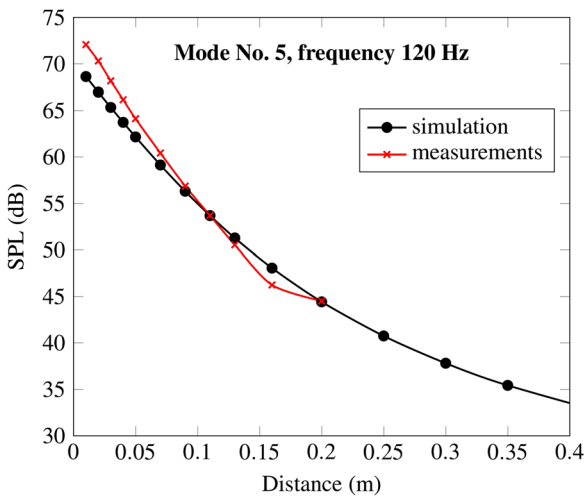

Fig. 3 Sound pressure level as a function of the distance in the *z*-axis from the center of the investigated plate structure vibrating in the fifth mode: numerical simulation and measurements

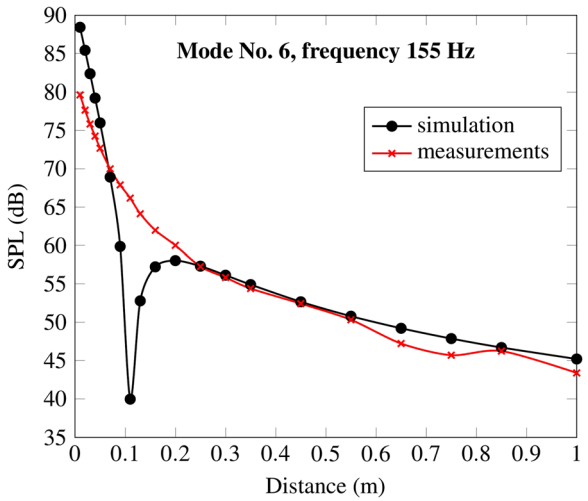

Fig. 4 Sound pressure level as a function of the distance in the *z*-axis from the center of the investigated plate structure vibrating in the sixth mode: numerical simulation and measurements

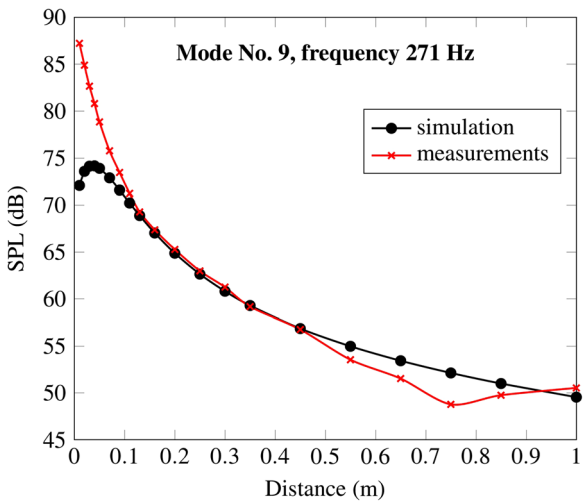

Fig. 5 Sound pressure level as a function of the distance in the *z*-axis from the center of the investigated plate structure vibrating in the ninth mode: numerical simulation and measurements

microphone by Brüel & Kjær (Nærum, Denmark, type 4193 with preamplifiers type 2664) connected to the Nexus 2690 conditioning amplifier, from the same manufacturer. The output of the amplifier was connected to an oscilloscope (Tektronix, Beaverton, OR, TDS 2004C).

The amplitude of the acoustic pressure was measured along the axis perpendicular to the surface of the plate and passing through its center and in several planes parallel to the plate's surface for different excitation frequencies equal to several selected eigenfrequencies of vibrations. The results of the measurements are presented in Figs. 3–9. Figures 3–6 present computed and measured sound pressure level values in the z-axis as functions of the distance from the center point of the plate. The measurements were taken at distances varying from 1 cm to 1 m. However, in case of the fifth structural mode (Fig. 3), the maximum range was shortened to 20 cm due to the low level of the observed amplitude of acoustic pressure. Figures 7–9 present computed and measured sound pressure level values in the plane $z = 2$ cm. The surface graphs illustrate the results of the numerical simulations, while the circles show values measured experimentally in the corresponding points of space.

One should notice that to compute the correct, absolute values of the acoustic pressure the normal velocity values introduced as the boundary conditions in the IVBEM model (see Eq. (2)) should correspond to the true normal velocity amplitudes of the vibrations excited during experiments. However, by solving the eigenproblem for an undamped system the velocity field is determined with accuracy of a scalar scaling factor. For that reason the results from the FEM model of plate vibrations have been scaled to the maximum amplitudes of velocities measured using the laser vibrometer for each vibrational mode, with specified excitation conditions.

The comparison of the measured and computed results reveals fair agreement between the experiments and numerical predictions. The computed distribution of the sound pressure level in the ambient space and the values of the amplitude of acoustic pressure have been largely proved correct. However, some significant discrepancies between simulations and measurements may be also observed (especially see Figs. 4 and 5). The errors result from imperfections in both laboratory stand (worse low-frequency performance of the anechoic chamber, propagation of vibrations through fastening elements, sound reflections from measurement equipment) and the developed mechanical and acoustic numerical models (assumption of ideal boundary conditions and material

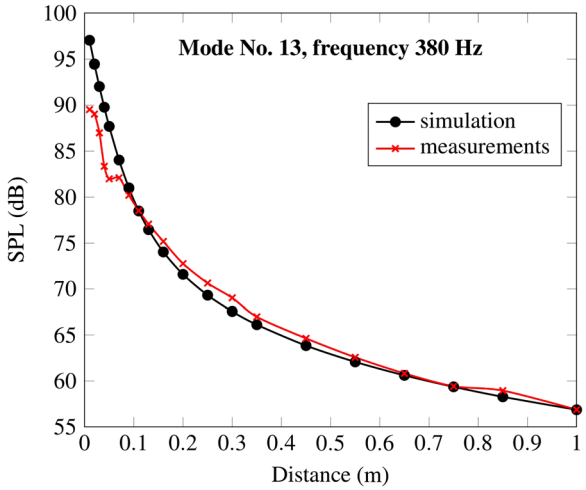

Fig. 6 Sound pressure level as a function of the distance in the *z*-axis from the center of the investigated plate structure vibrating in the thirteenth mode: numerical simulation and measurements

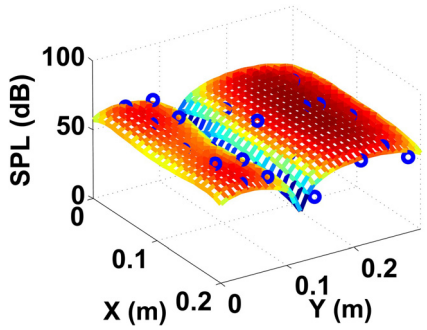

Fig. 7 The distribution of sound pressure levels (dB) in the plane $z = 2$ cm for vibrational mode no. 5 with frequency $f = 120$ Hz. The surface graph illustrates the results of the numerical simulations, while the circles show values measured experimentally in corresponding points of space.

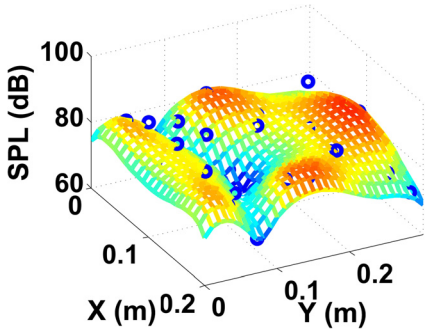

Fig. 8 The distribution of sound pressure levels (dB) in the plane $z = 2$ cm for vibrational mode no. 9 with frequency $f = 269$ Hz. The surface graph illustrates the results of the numerical simulations, while the circles show values measured experimentally in corresponding points of space.

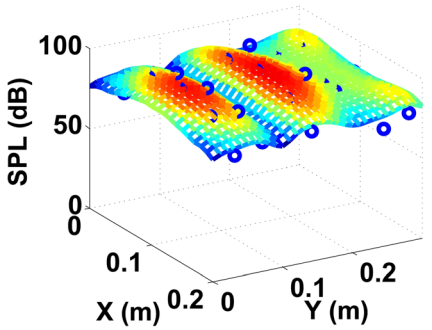

Fig. 9 The distribution of sound pressure levels (dB) in the plane $z = 2$ cm for vibrational mode no. 11 with frequency $f = 320$ Hz. The surface graph illustrates the results of the numerical simulations, while the circles show values measured experimentally in corresponding points of space.

properties, disregarding the influence of the piezoelectric transducers and electrical connections attached to the surface of the plate). The accuracy of the simulations can be probably further increased by improving the described issues.

The agreement between values obtained numerically and experimentally in general improves with the distance from the plate. This effect is caused by the fact that the complex character of the sound field distribution in the near-field zone promotes the intensification of errors caused by the mentioned imperfections. The results of the measurements carried out in *XY*-plane, 2 cm from the surface of the plate (Figs. 7–9) generally well agree with the computations. Significant discrepancies reaching up to few dB are observed in several isolated points (especially close to the edges), but the character of the distribution of sound pressure level in the immediate vicinity of the structure is in all cases reflected correctly. The numerical predictions become most reliable at distances greater than about 10–20 cm from the surface of the considered structure. Beyond this range about 6 dB drop in sound pressure level with doubling the distance is observed (see Figs. 4–9). This corresponds to the free-field spherical wave propagation.

5 Conclusions

The developed algorithm for determination of the free-field acoustic radiation characteristics of the vibrating plate structures with arbitrary boundary conditions has been described in the paper. The algorithm is based on the IVBEM and takes advantage of the features of simple geometry of the considered problem to optimize the computational time and cost. The presented results of numerical simulations, compared to the results of experimental investigations performed in an anechoic chamber prove high efficiency of the proposed method.

Modeling of the acoustic radiation of vibrating plate structures is an important practical problem, as it concerns lots of real-world technical applications such as machinery or cabin interior noise. Among a variety of numerical methods capable of handling the problem, the boundary element method is distinguished by reduction of the discretized domain to the plate's surface only and by ease of dealing with unbounded character of considered environment. However, exterior acoustic problems with open boundary surfaces require utilization of the variational computational scheme, which introduces double surface integrals with highly singular integrands. The present paper shows that in the considered case the resulting equations may be effectively solved in reasonable time.

The comparison between the results of numerical simulations and experiments performed in an anechoic chamber revealed good agreement between the obtained values of predictions and measurements, however some significant discrepancies in the near-field zone, at distances lower than about 10–20 cm from the surface of the plate were also observed. This effect is caused by the fact that the complex character of the sound field distribution close to the vibrating plate enhances the negative impact of both imperfections in laboratory stand and idealized model assumptions. At greater distances the agreement between results may be regarded as satisfactory. Taking into account the described

limitations, the developed algorithm may be regarded as a useful and effective tool in analysis of free-field acoustic radiation characteristics of vibrating plate structures with arbitrary boundary conditions.

Acknowledgment

The first author would like to acknowledge the financial support of the National Science Centre within the framework of his Ph.D. project—Project "Adaptive Composite Noise Absorbers," No. UMO-2011/01/N/ST8/07755. The second author would like to acknowledge the financial support of the Structural Funds in the Operational Program—Innovative Economy (IE OP), financed from the European Regional Development Fund—Project "Modern Material Technologies in Aerospace Industry," No. POIG.0101.02-00-015/08.

References

[1] Fuller, C. R., 1985, "Experiments on Reduction of Aircraft Interior Noise Using Active Control of Fuselage Vibration," J. Acoust. Soc. Am., **78**(S1), p. S88.
[2] Fuller, C. R., 1987, "Apparatus and Method for Global Noise Reduction," U.S. Patent No. 4,715,559.
[3] Fuller, C. R., and Silcox, R. J., 1992, "Acoustics 1991: Active Structural Acoustic Control," J. Acoust. Soc. Am., **91**(1), p. 519.
[4] Hansen, C. H., and Snyder, S. D., 1991, "Effect of Geometric and Structural/Acoustic Variables on the Active Control of Sound Radiation From a Vibrating Surface," Conference on Recent Advances in Active Control of Sound and Vibration, Blacksburg, VA, Apr. 15–17, Vol. 1, pp. 487–505.
[5] Thi, E. U., and Zuniga, M., 1991, "Comparison of Design Approaches in Sound Radiation Suppression," Conference on Recent Advances in Active Control of Sound and Vibration, Blacksburg, VA, Apr. 15–17, Vol. 1, pp. 15–17.
[6] Thomas, D. R., Nelson, P. A., and Elliott, S. J., 1990, "Experiments on the Active Control of the Transmission of Sound Through a Clamped Rectangular Plate," J. Sound Vib., **139**(2), pp. 351–355.
[7] Baumann, W. T., Saunders, W. R., and Robertshaw, H. H., 1991, "Active Suppression of Acoustic Radiation From Impulsively Excited Structures," J. Acoust. Soc. Am., **90**(6), pp. 3202–3208.
[8] Nowak, L. J., and Zieliński, T. G., 2013, "Modal Sensitivity and Selectivity of Small, Rectangle-Shaped Piezoelectric Transducers Used as Sensors and Actuators in Active Vibroacoustic Control Systems," J. Low Freq. Noise Vib. Act. Control, **32**(4), pp. 253–272.
[9] Fuller, C. R., Elliot, S. J., and Nelson, P. A., 1996, *Active Control of Vibration*, Academic Press, London.
[10] Maidanik, G., and Kerwin, E. M., 1966, "Influence of Fluid Loading on the Radiation From Infinite Plates Below the Critical Frequency," J. Acoust. Soc. Am., **40**(5), pp. 1034–1038.
[11] Stuart, A. D., 1976, "Acoustic Radiation From Submerged Plates. I. Influence of Leaky Wave Poles," J. Acoust. Soc. Am., **59**(5), pp. 1160–1169.
[12] Stuart, A. D., 1976, "Acoustic Radiation From Submerged Plates. II. Radiated Power and Damping," J. Acoust. Soc. Am., **59**(5), pp. 1170–1174.
[13] Leniowska, L., 1997, "Acoustic Power of Fluid-Loaded Circular Plate Located in Finite Baffle," Arch. Acoust., **22**(4), pp. 423–435.
[14] Nelisse, H., Beslin, O., and Nicolas, J., 1998, "A Generalized Approach for the Acoustic Radiation From a Baffled or Unbaffled Plate With Arbitrary Boundary Conditions, Immersed in a Light or Heavy Fluid," J. Sound Vib., **211**(2), pp. 207–225.
[15] Nowak, Ł., and Zieliński, T. G., 2012, "Acoustic Radiation of Vibrating Plate Structures Submerged in Water," Hydroacoustics, **15**, pp. 163–170.
[16] Malecki, I., 1964, *Theory of Waves and Acoustic Systems* (in Polish), PWN, Warszawa, Poland.
[17] Leissa, A. W., and Qatu, M. S., 2011, *Vibrations of Continuous Systems*, McGraw-Hill, New York.
[18] Zielinski, T. G., 2010, "Multiphysics Modeling and Experimental Validation of the Active Reduction of Structure-Borne Noise," ASME J. Vib. Acoust., **132**(6), p. 061008.
[19] Zielinski, T. G., Galland, M. A., and Ichchou, M. N., 2012, "Fully Coupled Finite-Element Modeling of Active Sandwich Panels With Poroelastic Core," ASME J. Vib. Acoust., **134**(2), p. 021007.
[20] Thompson, L. L., 2006, "A Review of Finite-Element Methods for Time-Harmonic Acoustics," J. Acoust. Soc. Am., **119**(3), pp. 1315–1330.
[21] Harari, I., 2006, "A Survey of Finite Element Methods for Time-Harmonic Acoustics," Comput. Methods Appl. Mech. Eng., **195**(13), pp. 1594–1607.
[22] Ihlenburg, F., 1998, *Finite Element Analysis of Acoustic Scattering*, Springer-Verlag, New York.
[23] Wu, H., Jiang, W., and Liu, Y., 2013, "Analyzing Acoustic Radiation Modes of Baffled Plates With a Fast Multipole Boundary Element Method," ASME J. Vib. Acoust., **135**(1), p. 011007.
[24] Harari, I., and Hughes, T. J., 1992, "A Cost Comparison of Boundary Element and Finite Element Methods for Problems of Time-Harmonic Acoustics," Comput. Methods Appl. Mech. Eng., **97**(1), pp. 77–102.
[25] Kopuz, S., and Lalor, N., 1995, "Analysis of Interior Acoustic Fields Using the Finite Element Method and the Boundary Element Method," Appl. Acoust., **45**(3), pp. 193–210.
[26] Desmet, W., 2012, "Boundary Element Method in Acoustics," International Seminar on Applied Acoustics (ISAAC 23)—Course on Numerical and Applied Acoustics Leuven, Belgium, Sept. 20–21, pp. 16–25.
[27] Jabłoński, P., 2003, *Metoda elementów brzegowych w analizie pola elektromagnetycznego* (*Finite Element Method in the Analysis of Electromagnetic Field*, in Polish), Wydawnictwo Politechniki, Czestochowskiej, Poland.
[28] Ciskowski, R. D., and Brebbia, C. A., 1991, *Boundary Element Methods in Acoustics*, Computational Mechanics Publications, New York.
[29] Gaul, L., Kögl, M., and Wagner, M., 2003, *Boundary Element Methods for Engineers and Scientists*, Springer-Verlag, Heidelberg.
[30] Kirkup, S., 2007, *The Boundary Element Method in Acoustics*, Integrated Sound Software, Hebden Bridge, UK.
[31] Alia, A., Souli, M., and Erchiqui, F., 2006, "Variational Boundary Element Acoustic Modelling Over Mixed Quadrilateral-Triangular Element Meshes," Commun. Numer. Methods Eng., **22**(7), pp. 767–780.
[32] Wang, W., and Atalla, N., 1997, "A Numerical Algorithm for Double Surface Integrals Over Quadrilaterals With a $1/R$ Singularity," Commun. Numer. Methods Eng., **13**(11), pp. 885–890.